Archaeointensity analysis and archaeomagnetic age constraints of Maya pottery from Chichén-Itzá and surrounding sites

Análisis de arqueointensidad y datación arqueomagnética de cerámica maya proveniente de Chichén-Itzá y zonas aledañas

Alejandro **Rodríguez-Trejo**[1,*], Luis Manuel **Alva-Valdivia**[2, †]

[1] Laboratorio de Paleomagnetismo, Instituto de Geociencias, Universidad Nacional Autónoma de México. Blvd. Juriquilla 3001, Campus UNAM, Juriquilla La Mesa, 76230, Juriquilla, Querétaro.

[2] Instituto de Geofísica, Universidad Nacional Autónoma de México, Circuito de la Investigación Científica s/n, Ciudad Universitaria, Alcaldía Coyoacán, 04510, Ciudad de México.

* Corresponding author:
(A. Rodríguez-Trejo) *alexrt@geociencias.unam.mx*

How to cite this article:
Rodríguez-Trejo, A., Alva-Valdivia, L.M., 2025, Archaeointensity analysis and archaeomagnetic age constraints of Maya pottery from Chichén-Itzá and surrounding sites: Boletín de la Sociedad Geológica Mexicana, 77(2), A200225. http://dx.doi.org/10.18268/BSGM2025v77n2a200225

Manuscript received: October 2, 2024
Corrected manuscript received: February 13, 2025
Manuscript accepted: February 20, 2025

Peer Reviewing under the responsibility of Universidad Nacional Autónoma de México.

ABSTRACT

The results of archaeointensity and magnetic property analyses are presented for 24 ceramic fragments collected from four archaeological sites in the Maya region: Chichén-Itzá, Flor de Mayo and San Pedro Cholul in Yucatán, Mexico and Busiljá-Chocoljá in Chiapas, Mexico. The samples span various periods of occupation in the Maya area, ranging from the Middle Preclassic to the Early Postclassic. The analysis of magnetic properties identified titanomagnetite, with varying titanium content, as the primary carrier of magnetization. Different magnetic phases were detected, with Curie temperatures ranging from 150 °C to 520 °C, determined through k-T curve experiments. Magnetic hysteresis experiments revealed saturation magnetization values between 150 mT and 300 mT, with coercivity values ranging from 4.2 mT to 9.6 mT. The saturation remanence to saturation magnetization ratio (M_r/M_s) varied between 0.10 and 0.26, indicating a behavior characteristic of pseudo-single domain (PSD) grains. A total of nine archaeointensity values were obtained at the specimen level, ranging from 32 ± 3.2 μT to 67.6 ± 2.5 μT, with virtual axial dipole moment (VADM) values between 7.37 ZAm² and 14.84 ZAm². Additionally, four representative mean archaeointensity values were determined for the studied sites. The results are consistent with the expected values for the region and the estimated age of the materials, in agreement with available regional and global paleosecular variation models. Furthermore, four archaeomagnetic ages were estimated for the ceramic types analyzed across the different study sites, covering a period from the Middle Preclassic to the Terminal Late Classic. These estimations contribute to refining and constraining the previously assigned ages for each ceramic type based on its archaeological context.

Keywords: archeomagnetism, archaeointensity, Chichén-Itzá, paleomagnetism, geoarcheology, geophysics.

RESUMEN

Se presentan los resultados de arqueointensidad y propiedades magnéticas obtenidos a partir del análisis de 24 fragmentos cerámicos recolectados en cuatro sitios arqueológicos de la zona Maya: Chichén-Itzá, Flor de Mayo y San Pedro Cholul, en Yucatán, México, y Busiljá-Chocoljá, en Chiapas, México. Las muestras abarcan distintos periodos de ocupación en el área maya, desde el Preclásico Medio hasta el Posclásico Temprano. El análisis de las propiedades magnéticas identificó a la titanomagnetita, con diferentes contenidos de titanio, como el principal portador de la magnetización. Se detectaron distintas fases magnéticas con temperaturas de Curie que oscilan entre 150 °C y 520 °C, determinadas mediante experimentos de curvas k-T. Los experimentos de histéresis magnética muestran valores de saturación magnética entre 150 mT y 300 mT, con una coercitividad que varía entre 4.2 mT y 9.6 mT. El cociente de remanencia de saturación respecto a la magnetización de saturación (M_r/M_s) varía entre 0.10 y 0.26, lo que indica un comportamiento característico de pseudo-dominios simples (PSD). Se obtuvieron 9 valores de arqueointensidad a nivel espécimen, que varían entre 32 ± 3.2 μT y 67.6 ± 2.5 μT, con valores de momento dipolar axial virtual (VADM) comprendidos entre 7.37 ZAm² y 14.84 ZAm². Se obtuvieron 4 arqueointensidades medias representativas de los sitios estudiados. Los resultados obtenidos son consistentes con los valores esperados para la región y la edad esperada de los materiales, en concordancia con los modelos de variación paleosecular regionales y globales disponibles. Asimismo, se estimaron cuatro edades arqueomagnéticas correspondientes a los tipos cerámicos analizados en los distintos sitios de estudio, abarcando un periodo que va desde el Preclásico Medio hasta el Clásico Tardío Terminal. Estas estimaciones contribuyen a restringir y precisar las edades previamente asignadas a cada tipo cerámico en función de su contexto arqueológico.

Palabras clave: arqueomagnetismo, archaeointensidad, Chichén-Itzá, paleomagnetismo, geoarqueología, geofísica.

http://dx.doi.org/10.18268/BSGM2025v77n2a200225

1. Introduction

The spatial and temporal variations of the Earth's magnetic field (EMF), recorded in various geological and archaeological materials such as volcanic rocks, ceramics and sediments, facilitate the reconstruction of the secular behavior of the EMF over extended time periods. Globally, an increasing body of paleomagnetic and archaeomagnetic studies has contributed a substantial amount of directional and intensity data concerning the EMF from Holocene volcanic events and human occupation sites over the past 5,000 years. These data have enabled the development of global models that describe the paleosecular variation (PSV) of the EMF in different regions of the world. Models such as SHA.DIF.14K (Pavón-Carrasco *et al.*, 2014), CALS10k.2 (Constable *et al.*, 2016) and ArchKalmag14k (Schanner *et al.*, 2022), among others, offer insights into the secular variations of the EMF, with the precision of these models contingent upon the availability, quality and accuracy of regional data across specific time periods. Hence, the necessity for expanding the temporal and spatial scope of available data remains paramount.

Such models enable the construction of synthetic secular variation curves, which, among other applications, allow for the dating of volcanic and archaeological materials up to approximately 14,000 ka, by using specialized techniques (*e.g.*, Pavón-Carrasco *et al.*, 2011). The accuracy achieved with these methods is comparable to that obtained through radiometric dating techniques, such as radiocarbon dating (C_{14}).

In Mexico, several regional secular variation curves have been developed (*e.g.*, Goguitchaichvili *et al.*, 2018b; Mahgoub *et al.*, 2019; Hervé *et al.*, 2019, García-Ruiz *et al.*, 2021) based on paleomagnetic data from volcanic and archaeological materials originating from Mexico and Central America. Most of the data from volcanics and archeological materials, used for regional curves in Mexico and global models, are available on different databases such as LAPOD (Rodríguez-Trejo *et*

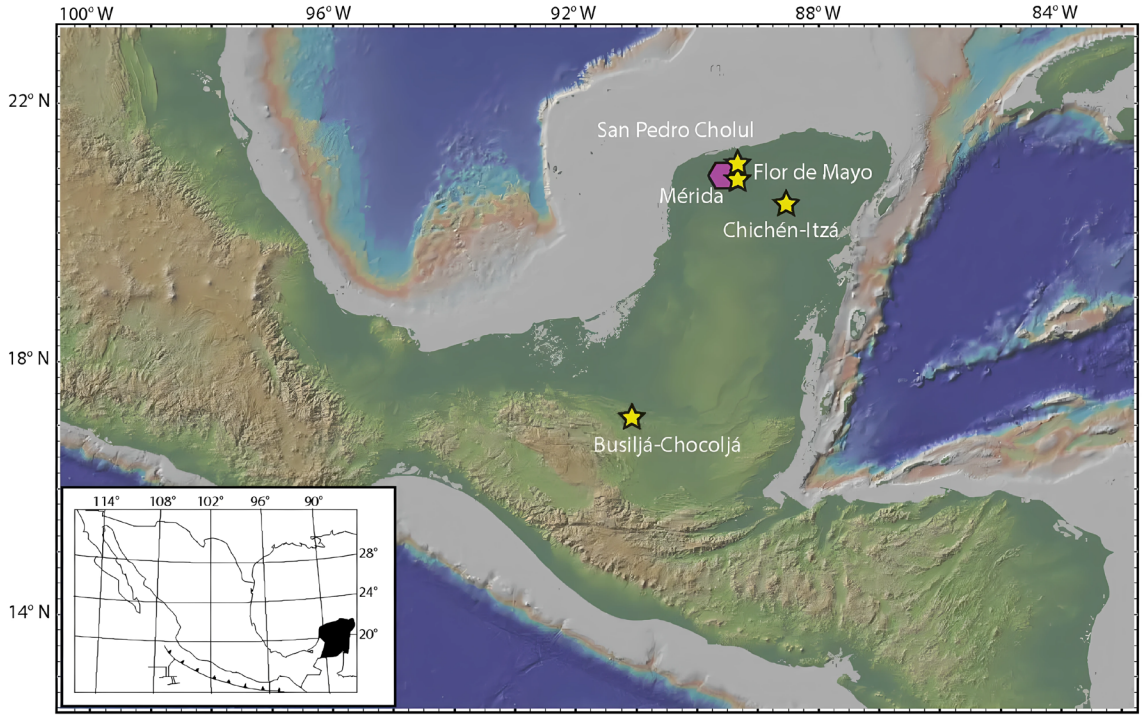

Figure 1 Location of the archaeological sites and the city of Mérida, Yucatán, Mexico.

http://dx.doi.org/10.18268/BSGM2025v77n2a200225

al., 2024). These models have been employed to date volcanic events and archaeological contexts, with their reliability and precision corroborated by numerous studies conducted across a variety of settings and time periods (*e.g.*, Böhnel *et al.*, 2016; Alva-Valdivia *et al.*, 2021; Rodríguez-Trejo *et al.*, 2023). Nonetheless, further data on the EMF's direction and intensity are required to enhance the quality and resolution of existing regional and global models. This expansion of the data set will allow for improved dating accuracy and a deeper understanding of the spatial and temporal behavior of the EMF.

This study presents archaeointensity results and magnetic properties' analysis of ceramic fragments from four archaeological sites located in the Yucatán Peninsula, Mexico (Figure 1), which correspond to the Maya civilization during distinct phases of Mesoamerican occupation (Figure 2). The Maya civilization was one of the most prominent and developed societies in Mesoamerica, occupying a vast area that extended over southern Mexico, Guatemala, El Salvador and Honduras. It had an almost continuous presence from approximately 2000 B.C.E. to the colonial period. In the region, different geophysical studies have been conducted with the aim of achieving a non-invasive survey of the different archaeological zones, including Chichén-Itzá (*e.g.*, Tejero-Andrade *et al.*, 2019; Cárdenas-Soto *et al.*, 2024). Archaeomagnetic studies have also been carried out in the region and generally in the Maya area, where data from archaeological materials such as kilns, ceramics and burnt soils, among others, have been obtained (*e.g.*, Alva-Valdivia *et al.*, 2021; Goguitchaitchvili *et al.*, 2018a, 2020; Ortiz-Ruiz *et al.*, 2024).

The chronology used for the sites in this study spans portions of the Preclassic (2500 B.C.E.–200 A.D.), Classic (200 A.D.–900 A.D.) and Postclassic (900 A.D.–1521 A.D.) periods, based on archaeological context and stratigraphy. In addition, four archaeomagnetic dating were conducted to accurately determine the age of each period. Ceramics and their associated

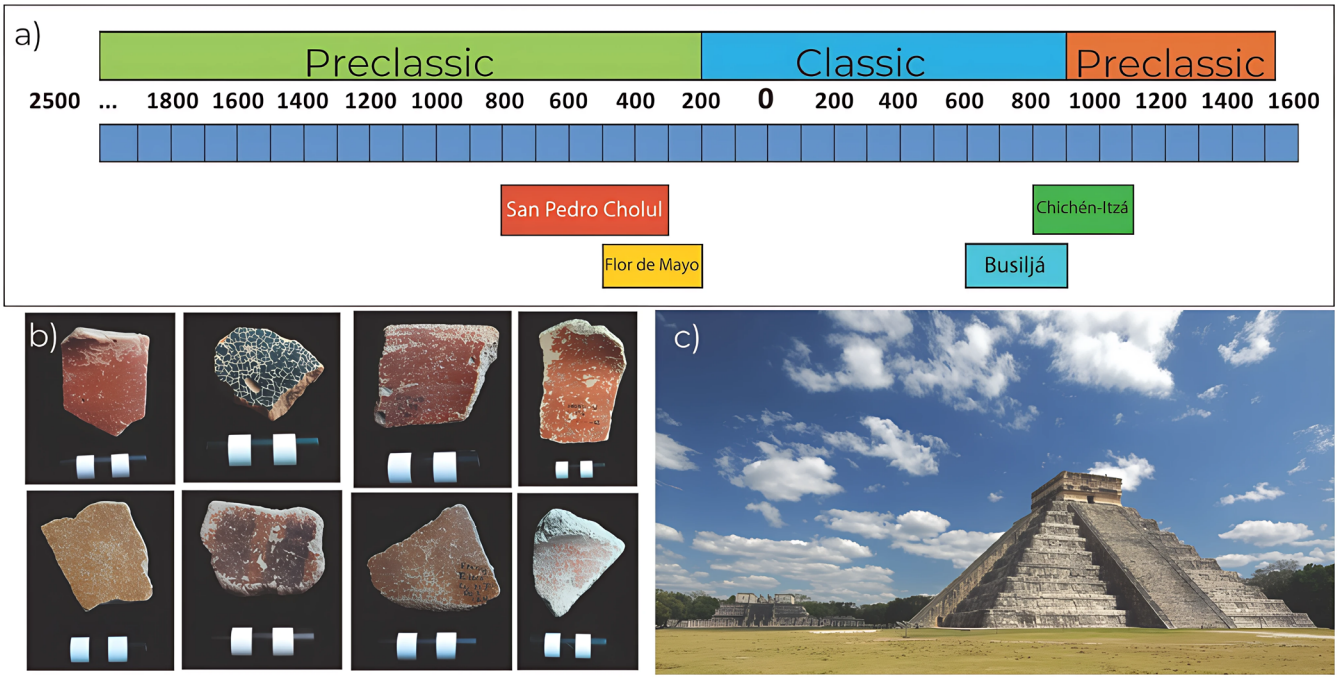

Figure 2 a) Chronological framework of the pottery sherds and archaeological sites, spanning from 2500 B.C.E. to 1600 A.D.; b) Representative pottery sherds analyzed in this study; c) The Temple of Kukulcán, Chichén-Itzá (image modified from www.inah.gob.mx).

http://dx.doi.org/10.18268/BSGM2025v77n2a200225

chronological relationships were provided by archaeologists from the Universidad Autónoma de Yucatán, drawing on research projects carried out at the sites of Chichén-Itzá, Flor de Mayo, San Pedro Cholul and Busiljá-Chocoljá. The dating of these materials was established through an analysis of each site's archaeological context, including known occupation periods, stratigraphy and the typological sequence of the recovered fragments. Each ceramic piece was retrieved from the same stratigraphic level as its corresponding dated context, thereby ensuring temporal consistency. Additionally, the samples correspond to six different ceramic types: Dzitas Pizarra (*e.g.*, Cobos 2001), Chinikiha (*e.g.*, Obando *et al.*, 2011), Sierra rojo (*e.g.*, Balcárcel *et al.*, 2010), Xanaba rojo (*e.g.*, Gallareta *et al.*, 2012), Juventud Rojo (*e.g.*, Quiñones-Cetina, 2006), and Chunhinta negro (*e.g.*, Rissolo *et al.*, 2005), which are associated with four distinct periods: Terminal Late Classic (700–1100 A.D.), Late Classic (600–900 A.D.), Late Preclassic (300 B.C.E.–250 A.D.), and Middle Preclassic (800–300 B.C.E.). Table 1 show the age period associated to each sample; general chronology is displayed in Figure 2.

2. Methodology

This study encompasses 24 ceramic sherds from four different archaeological sites (Figure 1). Each sherd was divided into 6 to 8 small fragments for the archaeointensity protocol (Figure 3a and 3b). Magnetic properties of the samples were measured at the Paleomagnetism Laboratory of the Institute of Geophysics, UNAM. A small fragment from each ceramic piece was selected for magnetic susceptibility as a function of temperature (k-T) measurements, utilizing an MFK2 susceptibility-meter (Agico, Kappabridge). The fragments were ground into powder and heated from room temperature to a maximum of

Figure 3 a) Sample assembly in salt cylinders (2.5 cm in diameter); b) Mounting of samples in a high-temperature-resistant diamagnetic plaster matrix; c) Sample holder used for heating samples embedded in salt; d) JR-6 spin magnetometer at IGF-UNAM; e) 2G cryogenic magnetometer at CEREGE-CNRS.

http://dx.doi.org/10.18268/BSGM2025v77n2a200225

Table 1. Summary of reported archaeointensity results, including their associated ceramic type and the age period estimated by typology.

Specimen	Period	Ceramic type	Site
MAYAS02	Terminal Late Classic 700–1100 A.D.	Dzitas Pizarra	Chichén-Itzá
MAYAS06	Terminal Late Classic 700–1100 A.D.	Dzitas Pizarra	Chichén-Itzá
MAYAS08	Terminal Late Classic 700–1100 A.D.	Dzitas Pizarra	Chichén-Itzá
MAYAS09	Late Classic 600–900 A.D.	Chinikiha	Busljá-Chocoljá
MAYAS10	Late Classic 600–900 A.D.	Chinikiha	Busljá-Chocoljá
MAYAS05	Late Preclassic 300 B.C.E.–250 A.D.	Sierra rojo	Flor de Mayo
MAYAS14	Late Preclassic 300 B.C.E.–250 A.D.	Xanaba rojo	Flor de Mayo
MAYAS11	Middle Preclassic 800–300 B.C.E.	Joventud Rojo	San Pedro Cholul
MAYAS16	Middle Preclassic 800–300 B.C.E.	Chunhinta negro	San Pedro Cholul

620 °C. The heating and cooling processes were conducted in an Argon atmosphere to minimize oxidation effects during thermal treatment. For the magnetic hysteresis and isothermal remanent magnetization (IRM) experiments, a fragment of approximately 25 mg from each ceramic piece was sectioned. The measurements were conducted using a Princeton 2900 MicroMag Alternating Gradient Magnetometer (AGM), applying a maximum magnetic field of 1.2 Tesla.

To determine archaeointensity, the samples were processed at both the Rock Paleomagnetism Laboratory of the Institute of Geophysics, UNAM and the Paleomagnetism Laboratory of CEREGE-CNRS & Aix-Marseille University, France. The double-heating protocol proposed by Thellier and Thellier (1959) was employed, wherein each sample is subjected to two thermal cycles while a laboratory magnetic field is applied along the +Z and -Z axes. During the experiments, partial thermo-remanent magnetization (pTRM) checks (Coe, 1967) were performed after every two temperature steps to verify potential magnetic mineralogical alterations during heating. The samples were heated in magnetically shielded rooms at both UNAM (67% of the samples) and CEREGE-CNRS (33% of the samples), with temperature increments ranging from 200 °C to 580 °C, while applying a magnetic field of 40 μT. The remanent magnetization was measured using an AGICO JR-6 spinner magnetometer at UNAM and a 2G Enterprises cryogenic magnetometer at CEREGE-CNRS. Data processing and interpretation were performed using the web-based application paleointensity.org (Beguin *et al.*, 2020) and the software ThellierTool 4.22 (Leonhardt *et al.*, 2004).

Given the nature of general ceramic manufacturing, anisotropic thermoremanent magnetization (ATRM) may occur, potentially introducing biases in archaeointensity estimates (Rogers *et al.*, 1979; Aitken *et al.*, 1988), often leading to overestimations or underestimations of intensity values. To mitigate this effect, it is essential to correct for anisotropy by calculating the ATRM tensor (Veitch *et al.*, 1984; Chauvin *et al.*, 2000). This correction involves four additional heating steps as part of the Thellier-Thellier procedure, using the final temperature of the heating process. Successive measurements are performed along six sample orientations corresponding to the +x, −x, +y, −y, +z, and −z axes. The last two measurements include the final heating step of the Thellier-Thellier process, followed by a thermal alteration check.

The anisotropy correction was applied individually to each specimen, with a correction factor for ATRM estimated for each sample, following the methodologies outlined by Veitch (1984) and Chauvin *et al.* (2000).

http://dx.doi.org/10.18268/BSGM2025v77n2a200225

3. Results

3.1. MAGNETIC PROPERTIES

3.1.1. MAGNETIC SUSCEPTIBILITY AS A FUNCTION OF TEMPERATURE (K-T)

The curves obtained from the k-T experiments were classified into two groups according to their reversible behavior and similar Curie temperature (Tc), as shown in Figure 4. The first group, which represents 25% of the specimens, shows two magnetic phases: the first between 320 °C and 370 °C (Figure 4a) and another between 450 °C and 520 °C. The second group, corresponding to 75% of the specimens, also exhibits two or more magnetic phases, the first between 150 °C and 180 °C (Figures 4b, 4c and 4d), and another between 400 °C and 450 °C. In both groups, the predominant magnetic carrier is associated with a transition between Ti-rich and Ti-poor titanomagnetites.

In 90% of the results, a low level of reversibility is observed, where cooling curves show susceptibility values that increase by up to 300% compared to the heating curve. This indicates significant mineralogical alteration during the heating process, with the formation of new magnetic minerals such as magnetite and other titanomagnetites with varying Ti content. The specimen with the greatest reversibility corresponds to the one shown in Figure 4d. In 25% of the cases, a small magnetic phase near 620 °C is detected, which could correspond to titanohematite, possibly a product of alteration and oxidation during burial, along with exposure to moisture and pedogenic processes.

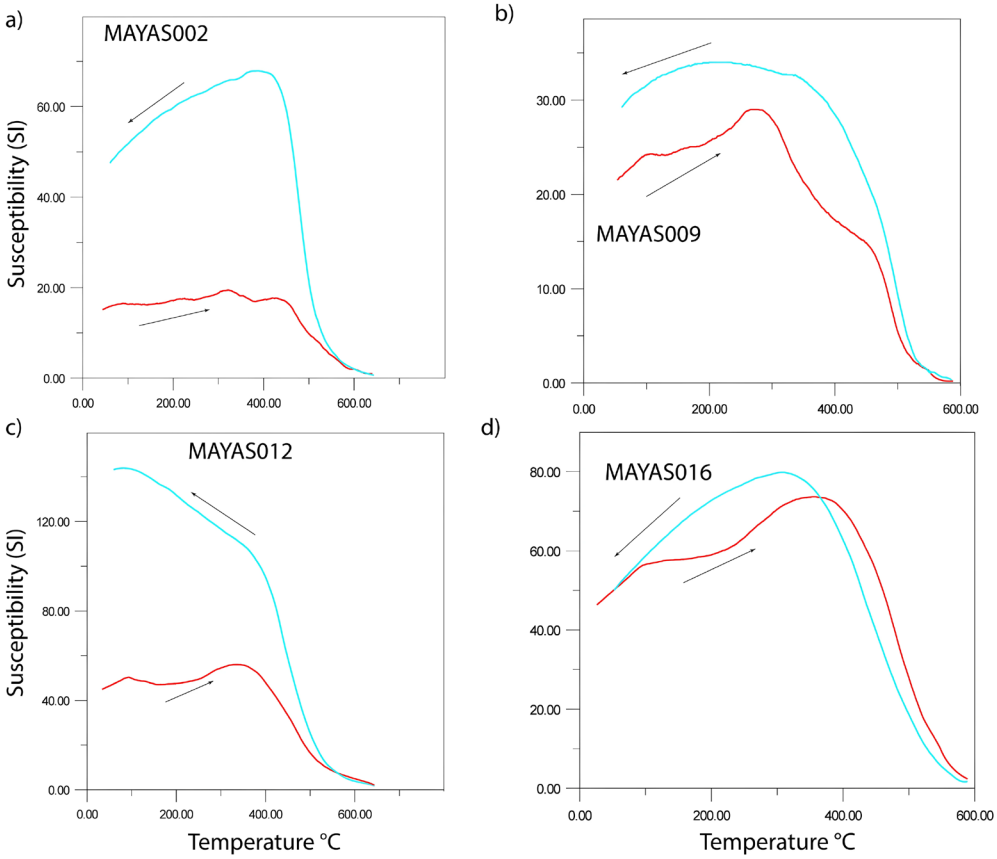

Figure 4 Summary of representative susceptibility vs. temperature experiments. The red curve represents the heating process, while the blue curve corresponds to the cooling process.

http://dx.doi.org/10.18268/BSGM2025v77n2a200225

3.1.2. MAGNETIC HYSTERESIS

The results of the magnetic hysteresis experiments reveal a diverse mixture of magnetic minerals. All measurements were normalized by specimen mass. In 80% of the samples, a characteristic *potbellied* behavior (Figures 5b, 5c and 5d) was observed, indicating predominantly pseudo-single domain (PSD) behavior, as described by Tauxe *et al.* (1996, 2002).

In the remaining specimens, a *wasp-waisted* behavior was identified, suggesting a mixture of minerals with both low and high coercivity, such as titanomagnetite and titanohematite (Figure 5a).

Saturation magnetization values range from 150 mT to 300 mT, coercivity values between 4.2 mT and 9.6 mT and squareness ratio values between 0.104 and 0.26 (M_{rs}/M_s). These values indicate a trend from small to medium-sized magnetic grains typical of PSD structures (Tauxe *et al.*, 2002), transitioning towards larger grains associated with multi-domain (MD) structures. This transition is evident in the Day plot (Day *et al.*, 1977), where a shift from PSD to MD particles is observed (Figure 6). Data from the Chichén-Itzá, San Pedro Cholul and Flor de Mayo sites show good clustering, while the Busiljá-Chocoljá site, located further from the Chichén-Itzá region, exhibits more variability.

Both the k-T and hysteresis curves confirm a consistent identification of the dominant magnetic mineralogy. The results indicate that the magnetic carriers are primarily titanomagnetite and magnetite, with lesser contributions from high-coercivity minerals such as titanohematite. The predominance of titanomagnetite and magnetite is evidenced in the k-T curves and further supported by the *potbellied* hysteresis loops. Similarly, the presence of titanohematite is corroborated by both the k-T curves and the wasp-waisted behavior observed in the hysteresis loops.

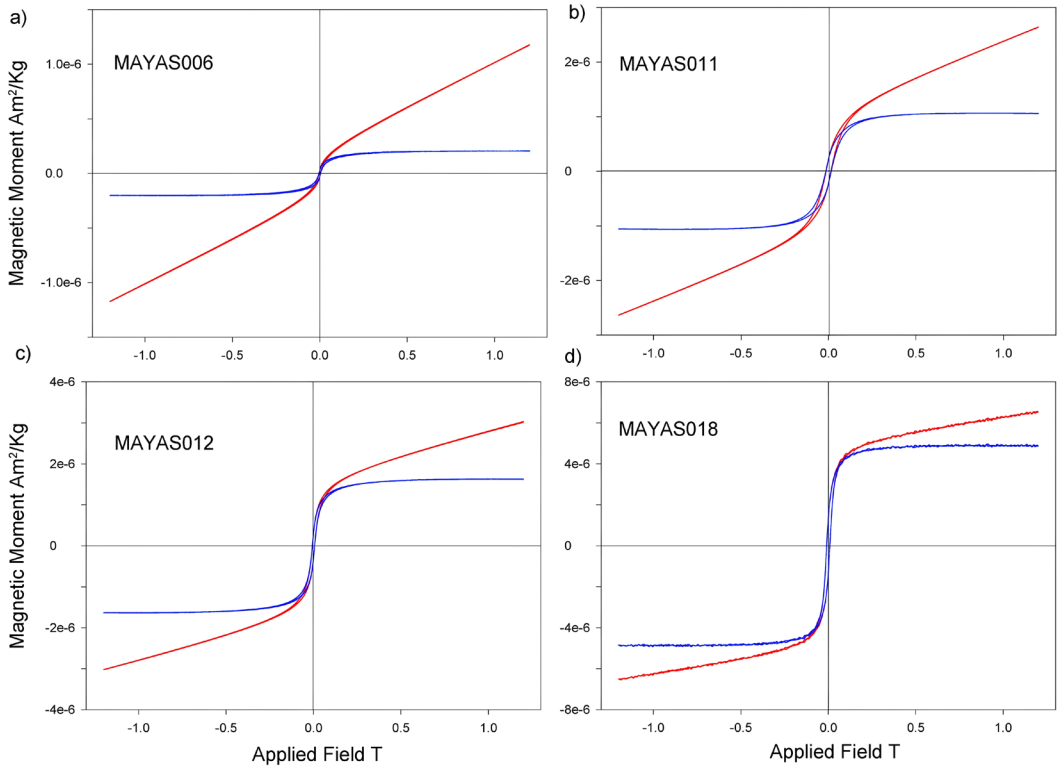

Figure 5 Summary of representative curves of magnetic hysteresis experiments. The curve in red shows the result of the mass normalized experiment. The blue curve shows the mass normalized results after correction for the contribution of paramagnetic mineralogy.

http://dx.doi.org/10.18268/BSGM2025v77n2a200225

3.2. ARCHAEOINTENSITY

The preparation of ceramic pieces followed two different methodologies. In the paleomagnetism laboratory at UNAM, 16 out of 24 ceramic pieces were processed. Each piece was cut into six cubic fragments (5 mm per side), which were embedded in a diamagnetic matrix of powdered salt. The fragments were then compacted under pressure into 2.5 cm diameter cylinders (Figures 3a, 3c and 3d). In the paleomagnetism laboratory at CEREGE-CRNS, 8 out of 24 ceramic pieces were processed, cutting six fragments from each piece, shaped as parallelepipeds of 5x3x15 mm, and embedded in a matrix of a high-temperature-resistant diamagnetic gypsum compound (Figures 3b and 3e).

Archaeointensity experiments were conducted on 144 specimens obtained from 24 ceramic fragments across four archaeological sites (Figure 1). To ensure the reliability of the results, eleven quality criteria were established based on the parameters proposed by Paterson *et al.* (2014) and the acceptance standards described for the ThellierTool software (Leonhardt *et al.*, 2004).

The number of heating steps (n) used to calculate the best-fit linear segment in the Arai-Nagata diagram (Nagata *et al.*, 1965) must be at least 5. The standard error ratio (β) should remain below 0.15, while the fraction (f), representing the proportion of total thermoremanent magnetization (TRM) included in the linear fit, must exceed 35%. Additionally, the gap factor (g), which evaluates the uniformity of temperature intervals, needs to be greater than 0.5 and the quality factor (q), reflecting the overall reliability of the fit, must be higher than 3.

The maximum angular deviation (MAD), as defined by Kirschvink (1980), should not surpass 10°. Furthermore, δCK, which is the maximum absolute difference generated by partial TRM (pTRM) checks and normalized by the total TRM, is required to be less than 9%. The cumulative alteration parameter, δpal, determined by the difference between corrected and uncorrected intensity estimates, must be under 18%. The parameter |k'|, representing the inverse of the radius of the best-fit circle to the Arai plot data, should not exceed 0.27.

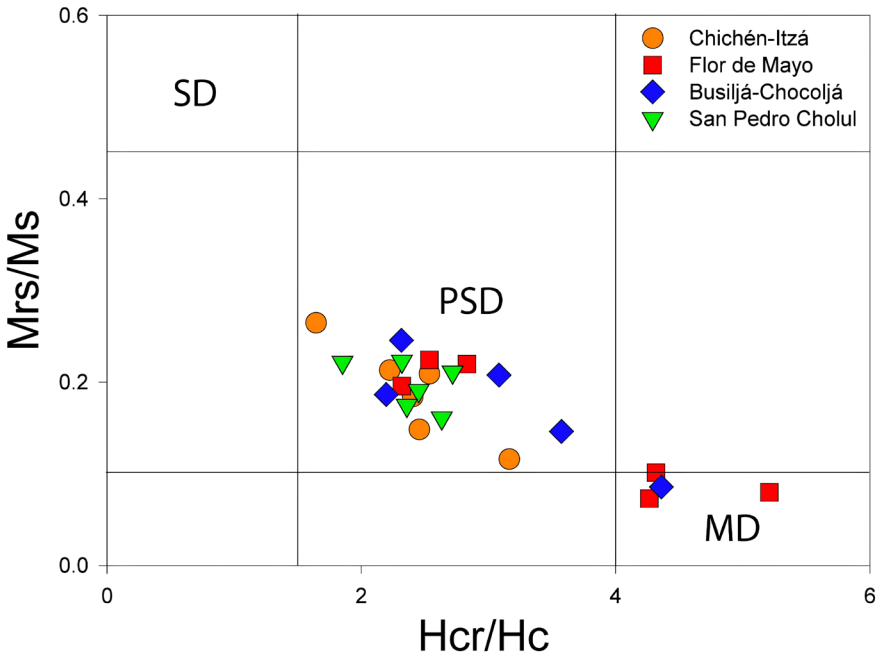

Figure 6 Day plot shows the results of magnetic properties (domain state) for each sherd, represented by an archaeological site.

http://dx.doi.org/10.18268/BSGM2025v77n2a200225

For each ceramic fragment, at least three specimens must yield valid results to calculate a reliable archaeointensity mean and the standard deviation (σ) of these values must not exceed 5 μT.

Based on the aforementioned criteria, reliable archaeointensity values were obtained for 30 out of 144 processed specimens (Table 2), representing up to 21% of the total samples. The remaining results were excluded from the final analysis for failing to meet the minimum parameters required to be considered valid for paleointensity estimates. In some cases (up to 25%), the results were discarded due to the presence of a strong secondary magnetization component (Figure 7d), likely caused by reheating or alteration processes. Additionally, approximately 50% of the samples were rejected because they did not meet all the established criteria for reliable archaeointensity determination. In all these cases, the specimens were disqualified from further analysis.

From the 30 archaeointensity measurements, 9 mean values were obtained for the four archaeological sites analyzed in this study. The intensity values ranged from 32 ± 3.2 μT to 67.6 ± 2.5 μT, while the virtual axial dipole moments (VADM) varied between 7.37 ZAm² and 14.84 ZAm² (Figure 7).

Table 2 presents the archaeointensity results that meet the established quality criteria. Each Banc value was corrected by multiplying it by its respective F_{ATRM}, yielding the intensity value corrected for anisotropy (B_{ATRM}). In most cases, the correction factor fell within the range of 1% < F_{ATRM} < 12%. This correction process refines the intensity estimates by reducing the anisotropy effect, which otherwise leads to overestimation or underestimation of the Earth's magnetic field (EMF) intensity in the analyzed samples.

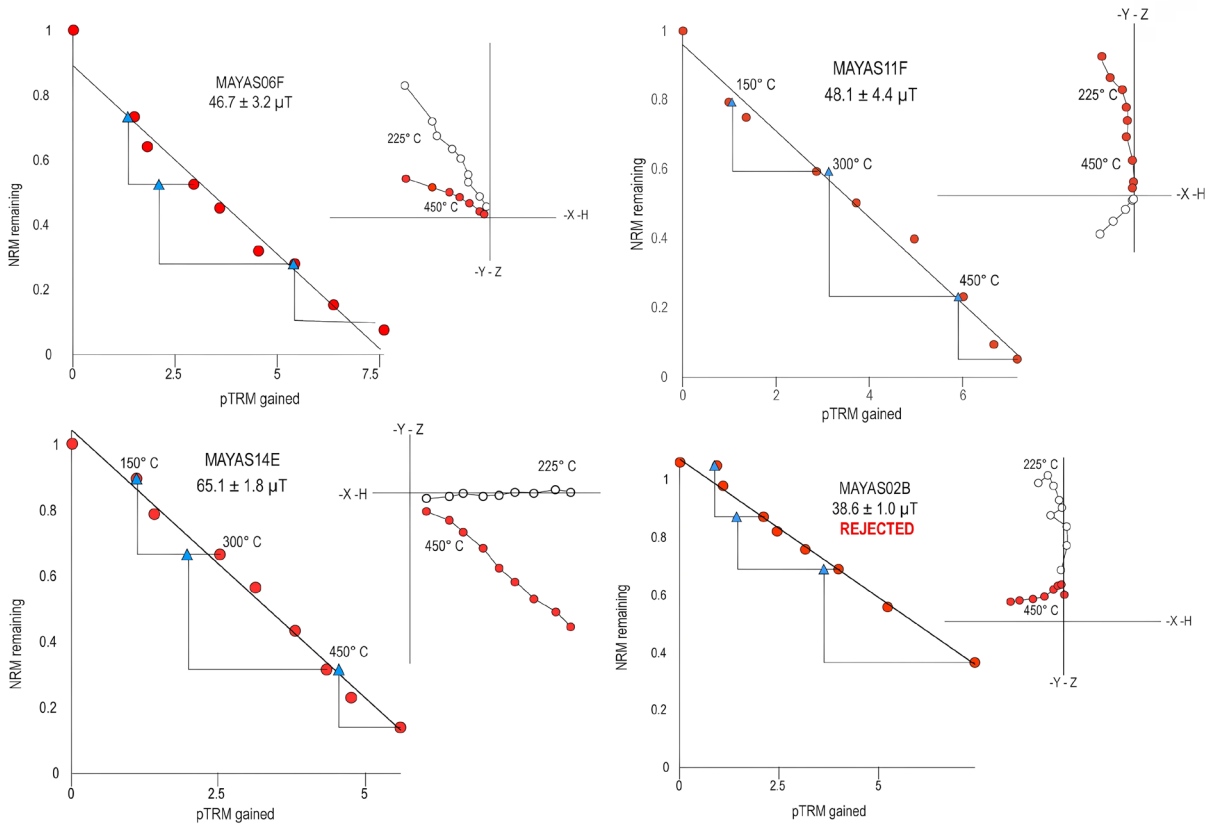

Figure 7 **Summary of representative archaeointensity results. Arai-Nagata plot with stability checks (on the left) and thermal demagnetization diagram (right).**

http://dx.doi.org/10.18268/BSGM2025v77n2a200225

Table 2. Summary of archaeointensity results. B_{lab}: Laboratory-applied field; Espec: Specimen; N: Number of points used to estimate the slope in the Arai-Nagata plots; f: Fraction of NRM; g: Gap factor; q: Quality factor; MAD: Maximum angle of deviation; β: Standard error ratio; Banc: Estimated archaeointensity in microtesla (μT); Bσ: Archaeointensity standard deviation; F_{ATRM}: Estimated correction factor for ATRM; B_{ATRM}: Archaeointensity corrected by the ATRM value; B_{CDMX}: Archaeointensity relocated to a reference location in central Mexico; VADM: Virtual axial dipole moment estimated in ZAm².

Site	Specimen	n	f	g	q	β	MAD_{Anc}	α	δCk	δpal	| k' |	B_{anc}	B_σ	F_{ATRM}	B_{ATRM}	B_{CDMX}	VADM	Class	Mean B	Estimated age
Chichén-Itzá	MAYAS02A	5	0.44	0.7	15	0.02	4	11.95	6.2	14.5	0.01	37.3	2	1.12	41.8	41	9.18	B		
Chichén-Itzá	MAYAS02D	6	0.48	0.74	16	0.022	3.4	9.52	6.3	9.6	0.04	35	1.1	0.981	34.3	33.7	7.54	A		
Chichén-Itzá	MAYAS02E	7	0.57	0.79	20	0.023	3.1	5.65	6.1	8.6	0.03	38.8	1.3	0.998	38.7	38	8.51	A		
Chichén-Itzá	MAYAS02F	8	0.61	0.81	11	0.044	3	10.07	6.6	9.6	0.25	42	2.2	1.06	44.5	43.7	9.78	A		
					Mean by sherd							**38.3**	**2.9**		**39.8**	**39.4**	**8.83**			
Chichén-Itzá	MAYAS06C	6	0.55	0.79	5	0.086	3.5	3.54	8.6	15.5	0.24	37.7	4.1	1.05	39.6	38.8	8.7	B		
Chichén-Itzá	MAYAS06D	7	0.69	0.82	10	0.06	4.1	2.46	7.3	17.5	0.045	37.4	4.5	0.995	37.2	36.5	8.18	B		
Chichén-Itzá	MAYAS06E	8	0.76	0.85	9	0.069	3.5	4.32	8.7	16.6	0.14	40.7	3.1	0.987	40.2	39.4	8.83	B	**39.8 ± 2.5**	**800–1100 A.D.**
Chichén-Itzá	MAYAS06F	9	0.99	0.85	11	0.08	3.8	2.11	7.8	17.6	0.21	42.7	3.2	0.908	42.4	41.6	9.32	B		
					Mean by sherd							**40.6**	**4.3**		**39.8**	**39.1**	**8.75**			
Chichén-Itzá	MAYAS08B	7	0.62	0.75	6	0.075	7.5	9.84	8.9	11.9	0.008	44.9		0.905	40.6	39.9	8.93	B		
Chichén-Itzá	MAYAS08E	8	0.69	0.79	10	0.057	6.9	10.24	7.8	14.7	0.12	47	3.5	0.943	44.3	43.5	9.74	B		
Chichén-Itzá	MAYAS08F	9	0.84	0.83	10	0.073	6.3	8.46	6.3	16	0.26	41.8	4.2	1.008	42.1	41.3	9.26	B		
					Mean by sherd							**44.6**	**2.6**		**42.4**	**41.5**	**9.31**			
Busiljá	MAYAS09A	4	0.5	0.51	5	0.049	5	9.83	5.2	16.9	0.134	34.2	1.2	1.091	37.3	38.3	8.58	B		
Busiljá	MAYAS09D	5	0.55	0.58	6	0.049	4.3	6.59	5.3	12.5	0.212	35.3	0.9	1.098	38.8	39.9	8.95	A		
Busiljá	MAYAS09C	6	0.55	0.57	4	0.074	4.2	7.22	6.4	14.8	0.047	33.9	2.2	1.09	36.95	38.1	8.54	B		
					Mean by sherd							**34.5**	**1.7**		**37.7**	**38.8**	**8.69**			
Busiljá	MAYAS10C	7	0.61	0.63	5	0.077	4.4	8.36	8.7	16.4	0.223	32.1	3.2	0.998	32.04	32.9	7.37	B	**37.7 ± 2.5**	**600–900 A.D.**
Busiljá	MAYAS10D	8	0.61	0.63	5	0.072	4.2	14.25	7.7	17.9	0.208	37.3	2.8	0.987	36.8	37.9	8.45	B		
Busiljá	MAYAS10F	9	0.62	0.63	6	0.064	4.2	12.92	8.8	17.6	0.268	38	2.4	0.997	37.9	39.1	8.74	B		
					Mean by sherd							**35.8**	**3.2**		**35.6**	**36.6**	**8.17**			
San Pedro Cholul	MAYAS05B	6	0.51	0.79	5	0.075	9.2	14.63	6.8	17.2	0.253	61.1	4	0.997	60.9	59.7	13.38	B		
San Pedro Cholul	MAYAS05C	7	0.64	0.83	10	0.056	9.6	13.5	7.7	17.3	0.054	58.5	3.7	0.978	57.2	56.1	12.57	B		
San Pedro Cholul	MAYAS05E	9	0.78	0.87	10	0.066	7.8	14.2	6.4	12.9	0.243	53.5	2.7	0.986	52.8	51.7	11.59	B		
					Mean by sherd							**57.7**	**3.2**		**56.8**	**56.1**	**12.01**			
San Pedro Cholul	MAYAS14C	6	0.48	0.8	7	0.052	3.3	5.06	8.9	9.1	0.201	72.2	4.7	0.89	64.3	63	14.12	A	**59.7 ± 4.2**	**300 B.C.E.–250 A.D.**
San Pedro Cholul	MAYAS14D	7	0.64	0.83	10	0.052	2.8	4.12	7.8	8.9	0.137	66.9	2.1	0.915	61.2	60	13.45	B		
San Pedro Cholul	MAYAS14F	8	0.71	0.85	15	0.04	2.9	4.35	8.7	8.3	0.043	67.9	2.5	0.995	67.6	66.2	14.84	B		
San Pedro Cholul	MAYAS14E	9	0.85	0.87	20	0.038	2.4	3.45	8.1	9.6	0.142	65.1	1.8	0.963	62.7	61.5	13.77	A		
					Mean by sherd							**68**	**3.1**		**63.9**	**62.7**	**14.05**			
Flor de Mayo	MAYAS11D	6	0.55	0.78	6	0.071	2	1.56	3.4	9.1	0.235	52.5	3.2	0.994	52.2	51.2	11.47	A		
Flor de Mayo	MAYAS11E	7	0.74	0.82	10	0.058	1.7	1.47	4.1	7.6	0.209	49.2	4.7	0.981	48.3	47.4	10.62	A		
Flor de Mayo	MAYAS11F	8	0.79	0.83	14	0.047	2.6	1.67	3.3	6.5	0.217	48.1	4.4	0.998	48	47.1	10.55	B		
					Mean by sherd							**49.9**	**2.3**		**49.5**	**48.6**	**10.9**			
Flor de Mayo	MAYAS16A	7	0.65	0.8	6	0.138	2.8	4.54	7.9	14.9	0.267	59.6	1.8	0.989	58.9	57.8	12.95	B	**53 ± 5.3**	**800–300 B.C.E.**
Flor de Mayo	MAYAS16B	8	0.69	0.81	5	0.105	3.4	5.9	8.3	13.9	0.236	60.8	2.1	0.995	60.5	59.3	13.29	B		
Flor de Mayo	MAYAS16E	9	0.73	0.83	6	0.098	3.4	6.06	7.7	13	0.147	56.6	4.3	0.998	56.5	55.4	12.41	B		
					Mean by sherd							**59**	**2.1**		**58.6**	**57.5**	**12.88**			

http://dx.doi.org/10.18268/BSGM2025v77n2a200225

Figure 9 compares the obtained results (Table 2) with two regional PSV curves (Mahgoub *et al.*, 2019; García-Ruiz *et al.*, 2021) and the global model SHA.DIF.14k (Pavón-Carrasco *et al.*, 2014). To facilitate this comparison, the B_{ATRM} results were relocated to a reference point in central Mexico at 19.43° N, 99.13° W, corresponding to Mexico City's center. These adjusted values are presented in Table 2, under the B_{CDMX} column.

A general agreement is observed between the archaeointensity values and the expected intensities from the PSV models, according to the estimated age of each sample. However, the archaeointensity results for the MAYAS05 specimen (Table 2) exhibit a maximum angle of deviation (MAD) between 5° and 10°, which is higher than that of the other specimens, where deviations remain below 5°. Despite this, the result meets the minimum acceptance criteria for archaeointensity studies.

3.3. ARCHAEOGMAGNETIC DATING

Archaeomagnetic dating was conducted using the MATLAB tool Archaeodating (Pavón-Carrasco *et al.*, 2011) in combination with the global geomagnetic models SHA.DIF.14k (Pavón-Carrasco *et al.*, 2014) and SHAWQ2k (Campuzano *et al.*, 2019), as well as the regional intensity PSV model (García-Ruiz *et al.*, 2021). The age estimation was performed within a chronological range spanning from 1500 B.C.E. to 1500 A.D (Figure 8).

For each sample, up to three age ranges were derived from the applied PSV models, in addition to the chronological constraints provided by the archaeological context associated with each ceramic type. To integrate these multiple estimates into a single representative age, a Bayesian approach was applied, incorporating the uncertainties associated with each interval. Bayesian inference is

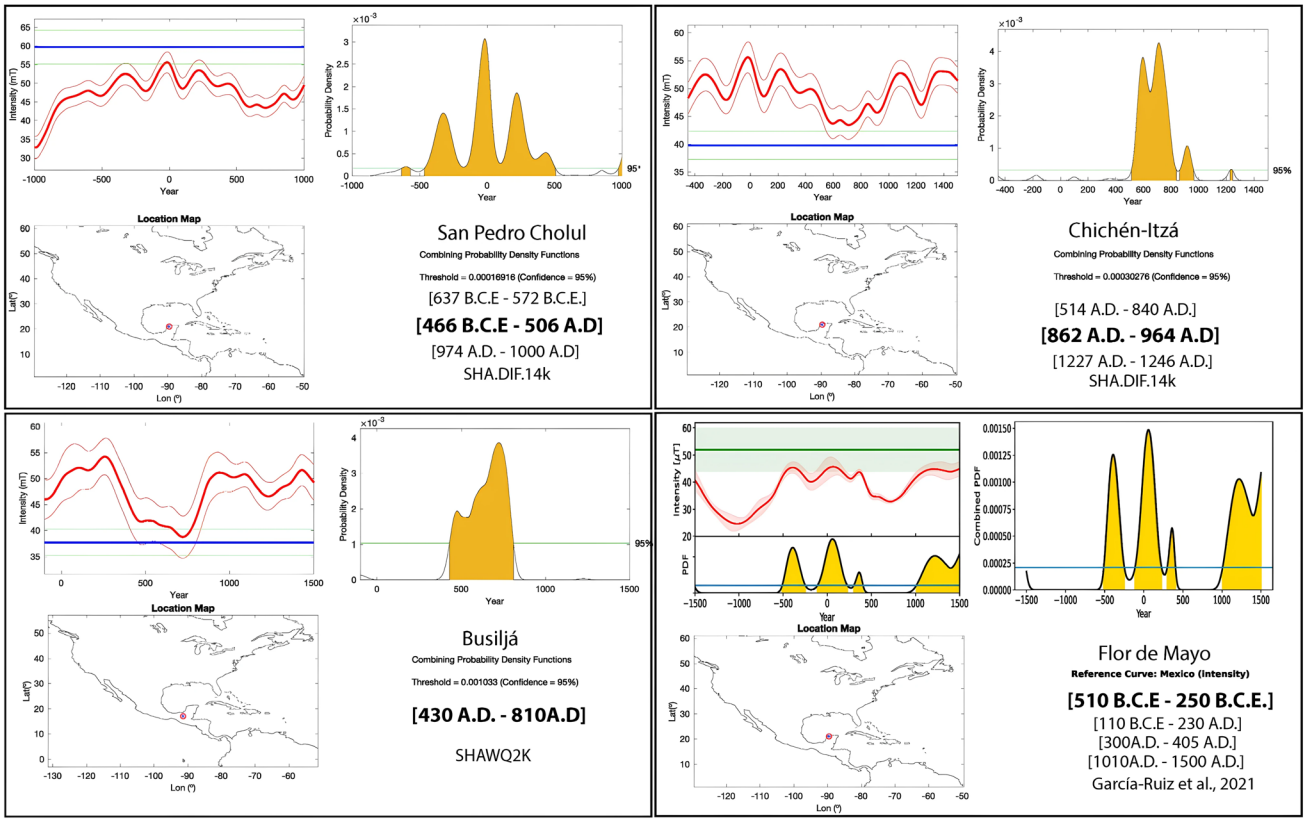

Figure 8 Archaeomagnetic dating results obtained using different PSV curves, analyzed with the Archaeodating MATLAB tool (Pavón-Carrasco *et al.*, 2014).

widely employed in chronological studies due to its ability to integrate prior knowledge and rigorously quantify uncertainty (Buck *et al.*, 1996; Gelman *et al.*, 2013).

For each given range (A_i,B_i), the central value was estimated as:

$$\mu_i = \frac{A_i + B_i}{2} \quad (1)$$

and the uncertainty was estimated:

$$\sigma_i = \frac{B_i + A_i}{4} \quad (2)$$

Assuming a uniform distribution within the interval. The final estimated age was derived through a weighted combination of the different sources based on their variances:

$$\mu_{post} = \frac{\sum_{i=1}^{N} \frac{\mu_i}{\sigma_i^2}}{\sum_{i=1}^{N} \frac{1}{\sigma_i^2}} \quad (3)$$

where μ_{post} represents the best estimate for the combined age. The posterior variance was estimated as:

$$\sigma_{post}^2 = \left(\sum_{i=1}^{N} \frac{1}{\sigma_i^2} \right)^{-1} \quad (4)$$

That quantifies the contribution of the uncertainty from each individual estimate and improves the precision of the final result (Gelman *et al.*, 2013). From these values, a 95% confidence interval was established using:

$$CI_{95\%} = \mu_{post} \pm 1.96 \cdot \sigma_{post} \quad (5)$$

providing a more reliable and statistically robust age range.

This method is particularly useful in chronological analysis when integrating data from different dating techniques or sources, as it allows for a probabilistic combination of independent estimates (Buck *et al.*, 1996). In the field of radiocarbon dating, Bayesian models have been extensively used to refine age determinations and to assess the consistency of different dating methods (Ramsey, 2009). After the Bayesian approach, 4 new ages were constrained based on the dating of the ceramic types, from the Middle Pre-Classic to the Terminal Late Classic. Table 3 summarizes the determined ages after the archaeomagnetic dating and the Bayesian inference.

4. Discussion

The results of the magnetic properties analysis reveal consistency in terms of the thermal and magnetic stability of the samples. The k-T curves predominantly display two distinct magnetic phases, characterized by high and low Curie temperatures. Additionally, the hysteresis curves indicate minimal magnetic mineralogical mixing, with saturation magnetization values remaining below 300 mT. The magnetic domain behavior primarily follows a pseudo-single domain (PSD) trend, with a minor component exhibiting multi-domain (MD) characteristics. These findings suggest that the dominant carriers of magnetization are titanomagnetites with varying titanium content.

The ratios of magnetization (M_{rs}/M_s) and coercivity (H_{cr}/H_c), as illustrated in the Day diagram, exhibit similar patterns across the Flor de Mayo, Chichén-Itzá and San Pedro Cholul archaeological sites. However, the results from Busiljá-Chocoljá show slight deviations.

One of the main limitations of existing global and regional paleosecular variation (PSV) models is the reliability of data reported in recent years. In some cases, paleomagnetic and archaeomagnetic data, both directional and intensity, fail to meet the minimum quality standards required for them to be considered reliable, introducing a significant source of error in the resulting models. Additionally, the dating of many samples often carries a high degree of uncertainty, and in some cases, chronological corrections or refinements are

http://dx.doi.org/10.18268/BSGM2025v77n2a200225

made over time, further increasing the uncertainty of the available models.

To ensure the reliability of the data, archaeointensity results were selected based on previously established quality criteria. An anisotropy effect was observed, directly associated with the ceramic manufacturing process. The ATRM correction improved the accuracy and precision of the results, revealing systematic overestimations in archaeointensity, which, on average, ranged between 5% and 10%.

The relocation of B_{CDMX} results to central Mexico enabled direct comparisons with PSV intensity curves from other regions of the country, such as those compiled by Mahgoub *et al.* (2019) and García-Ruiz *et al.* (2021), which primarily include records from central Mexico. Additionally, the results were compared with the global geomagnetic model SHA.DIF.14k (Pavón-Carrasco *et al.*, 2014). Despite the broad range of estimated ages, as shown in Figure 9, the obtained values remain within acceptable limits and align with the expected secular variation trends for the analyzed time period.

As observed in Figure 9, the values obtained in this study for the Late Classic period are consistent with the expected values from the PSV models presented. The result obtained for the Middle Preclassic period closely aligns with both the SHA.DIF.14k model and the reconstruction proposed by Mahgoub *et al.* (2019). In contrast, the estimated value for the Late Preclassic period shows a slight deviation from SHA.DIF.14k and Mahgoub *et al.* (2019), and a more marked discrepancy when compared with the model proposed by García-Ruiz *et al.* (2021). These discrepancies among the PSV models can be attributed to the limited availability of intensity data for this period (on all

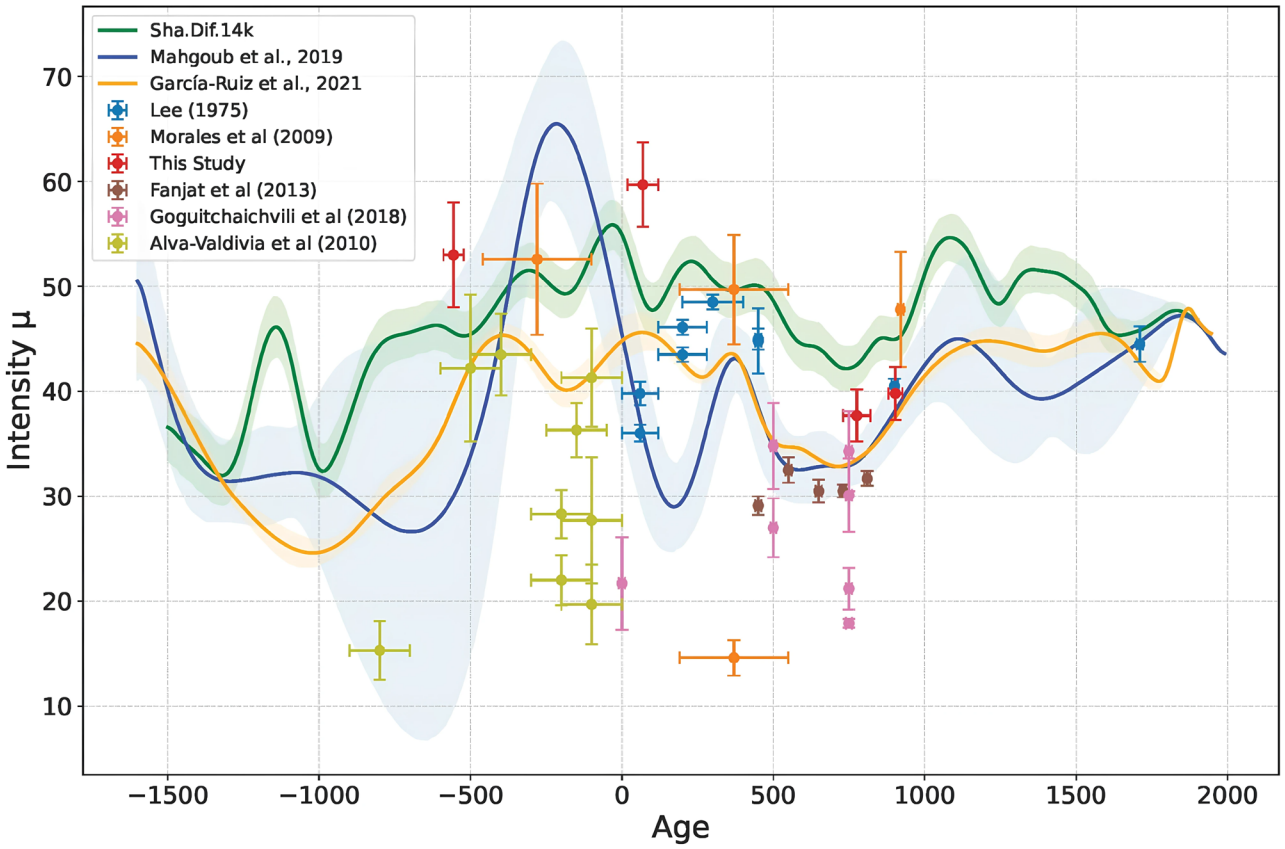

Figure 9 Comparison of archaeointensity results from this study with regional and global PSV models over the past 3,000 years.

Table 3. Summary of archaeomagnetic dating results based on different PSV curves, along with the estimated age using Bayesian inference.

Site	Estimated age range	PSV curve used for dating	Archaeomagnetic dating
Chichén-Itzá	800–1100 A.D.	Ceramic type dating	859–975 A.D.
	785–1165 A.D.	García-Ruiz *et al.*, 2021	
	426–809 A.D.	SHAWQ2K	
	862–964 A.D.	SHA.DIF.14k	
Busiljá-Chocoljá	600–900 A.D.	Ceramic type dating	689–864 A.D.
	795–1150 A.D.	García-Ruiz *et al.*, 2021	
	430–810 A.D.	SHAWQ2K	
	527–956 A.D.	SHA.DIF.14k	
Flor de Mayo	800–300 B.C.E.	Ceramic type dating	623–488 B.C.E.
	510–250 B.C.E.	García-Ruiz *et al.*, 2021	
	956–506 B.C.E.	SHA.DIF.14k	
San Pedro Cholul	300 B.C.E.–250 A.D.	Ceramic type dating	31 B.C.E.–170 A.D.
	85 B.C.E.–190 A.D.	García-Ruiz *et al.*, 2021	
	38 B.C.E.–364 A.D.	SHAWQ2K	
	466 B.C.E.–506 A.D.	SHA.DIF.14k	

the PSV models), which affects the robustness of the PSV curves.

Figure 9 also presents a comparison with previously published archaeointensity values from sites in the Maya region (*e.g.*, Lee, 1975; Morales *et al.*, 2009; Alva-Valdivia *et al.*, 2010; Fanjat *et al.*, 2013; Goguitchaichvili *et al.*, 2018a), revealing a pattern of both agreements and discrepancies with current PSV models. These inconsistencies emphasize the need to expand the available archaeointensity dataset to enhance the accuracy and resolution of PSV reconstructions for Mesoamerica. Data for comparison were obtained from LAPOD (Rodríguez-Trejo *et al.*, 2024).

5. Conclusions

The results obtained in this study provide valuable insights into the magnetic properties and archaeomagnetic dating of ceramic materials from four archaeological sites in the Maya region, which were occupied from the Middle Preclassic to the Early Postclassic period. These findings reveal similarities in the raw materials used for ceramic production, as well as in the magnetic mineralogy responsible for carrying the remanent magnetization, which enabled the archaeointensity analysis. The results confirm that the primary magnetic carriers are titanomagnetites with varying titanium content.

The Earth's magnetic field intensity values were selected based on strict quality criteria to ensure a high level of reliability. The archaeointensity results range from 32 ± 3.2 μT to 67.6 ± 2.5 μT, while the virtual axial dipole moment (VADM) values range from 7.37 ZAm² to 14.84 ZAm². These findings are consistent with expected values according to regional and global paleosecular variation (PSV) models for the last 3,000 years in Mexico.

The comparison of the results with regional and global PSV models highlights the need for further refinement of PSV curves for southeastern Mexico and Central America, a region rich in archaeological remains and Holocene volcanic materials but with limited published studies (*e.g.*, Alva-Valdivia *et al.*, 2010; Rodríguez-Trejo *et al.*, 2023). Therefore, the integration of paleomagnetic and archaeomagnetic data, including both intensity and directional records, combined with high-precision dating, is essential

for the development of more robust and refined PSV models for the region.

Additionally, the archaeomagnetic dating of four ceramic types from four archaeological sites provides valuable chronological constraints for each site. These results not only contribute to refining the archaeological context but also demonstrate the reliability and applicability of the paleomagnetic method as a chronological tool for Mesoamerican archaeology.

Contributions of authors

ART: Conceptualization, Data processing, Formal analysis, Methodology, Software analysis, data validation, Funding, Writing original draft preparation; LMAV: Material and samples acquisition, formal analysis, writing-review and editing.

Financing

This work was partially funded by UNAM-DGAPA fellowship 2020-2022. CONAHCyT for postdoctoral fellowship EPM 2022(1).

Acknowledgements

Thanks, and the deepest gratitude to Dr. Luis Manuel Alva Valdivia for all his teaching, patience, knowledge and above all, for his great friendship. This work honors your memory. Rest in peace, Doc. Alejandro Rodríguez-Trejo. Thanks to UNAM-DGAPA for the postdoctoral fellowship 2020-2022. ART also thanks CONAHCyT for the postdoctoral fellowship 2022 (1). Special thanks go to Socorro Jiménez-Álvarez, Alan Méndez Caab, Rafael Cobos, Charles Golden, and all archeologists from UADY and INAH for providing ceramic materials and their chronological relationships. Additional thanks to M.C. José Antonio González Rangel and Martín Espinoza for their technical support in the laboratory at the Geophysics Institute-UNAM, and to M.C. Héctor Ibarra for his assistance in figure preparation from the Geosciences Institute. Thanks to Ing. Jorge Escalante from Geosciences Institute for technical support. Thanks are also extended to Dr. Mireille Perrin and Dr. Gwenael Hervé for their support in the experimental work and for hosting at the Paleomagnetism Laboratory of CNRS-CEREGE.

Conflicts of interest

The authors declare that they have no known competing financial interests or personal relationships that could have appeared to influence the work reported in this paper.

Data availability

Data will be made available on request.

Handling editor

Avto Gogichaishvili.

References

Aitken M.J., Allsop, A.L., Bussell, G.D., Winter, M.B., 1988, Determination of the intensity of the Earth's magnetic-field during archaeological times – Reliability of the Thellier technique: Reviews of Geophysics, 26(1), 3–12. https://doi.org/10.1029/RG026i001p00003

Alva-Valdivia, L.M., Morales, J., Goguitchaichvili, A., De Hatch, M.P., Hernandez-Bernal, M.S., Mariano-Matías, F., 2010, Absolute geomagnetic intensity data from preclassic Guatemalan pottery: Physics of the Earth and Planetary Interiors, 180(1–2), 41–51. https://doi.org/10.1016/j.pepi.2010.03.002

Alva-Valdivia, L.M., Rodríguez-Trejo, A., Cruz-Antillón, R., Hervé, G., Perrin, M., Salgado-Saito, M.M., Mahgoub, A.N., 2021, Archaeomagnetic dating and magnetic characterization of ceramics from the

Paquimé, Casas Grandes region, Chihuahua, Mexico: Journal of Archaeological Science: Reports, 37, 103040. https://doi.org/10.1016/j.jasrep.2021.103040

Balcárcel, B., Shrodt, S., Hansen, R.D., Martínez, G., 2010, El último suspiro cerámico del Preclásico tardío en la Zona Cultura Mirador, Arroyo, B., Linares, A., Paiz, L., XXIII Simposio de Investigaciones Arqueológicas: Guatemala, Museo Nacional de Arqueología y Etnología, Guatemala, 1113–1127.

Béguin, A., Paterson, G.A., Biggin, A.J., de Groot, L.V., 2020, Paleointensity.org: An online, open source, application for the interpretation of paleointensity data: Geochemistry, Geophysics, Geosystems, 21(5), e2019GC008791. https://doi.org/10.1029/2019GC008791

Böhnel, H., Pavón-Carrasco, F.J., Sieron, K., Mahgoub, A.N., 2016, Palaeomagnetic dating of two recent lava flows from Ceboruco volcano, western Mexico: Geophysical Journal International, 207(2), 1203–1215. https://doi.org/10.1093/gji/ggw310

Buck, C.E., Cavanagh, W.G., Litton, C.D., Scott, M., 1996, Bayesian approach to interpreting archaeological data: Chichester, Wiley, 226–233.

Campuzano, S.A., Gómez-Paccard, M., Pavón-Carrasco, F.J., Osete, M.L., 2019, Emergence and evolution of the South Atlantic Anomaly revealed by the new paleomagnetic reconstruction SHAWQ2k: Earth and Planetary Science Letters, 512, 17–26. https://doi.org/10.1016/j.epsl.2019.01.050

Cárdenas-Soto, M., Sánchez-González, J., Martínez-González, J.A., Escobedo-Zenil, D., Sandoval-Quintana, O., Carrillo-Vargas, A., Argote-Espino, D.L., López-García, P.A., Cifuentes-Nava, G., 2024, Identificación de la respuesta sísmica en pirámides del área de Chichén Itzá para preservar el patrimonio cultural: Boletín de la Sociedad Geológica Mexicana, 76(2), A030324. http://dx.doi.org/10.18268/BSGM2024v76n2a020324

Chauvin, A., Garcia, Y., Lanos, Ph., Laubenheimer, F., 2000. Paleointensity of the geomagnetic field recovered on archaeomagnetic sites from France: Physics of the Earth and Planetary Interiors, 120(1–2), 111–136. https://doi.org/10.1016/S0031-9201(00)00148-5

Cobos, R., 2001, El centro de Yucatán: de área periférica a la integración de la comunidad urbana en Chichén Itzá, in Ciudad-Ruiz, A., Iglesias-Ponce de León, M.J., Martínez-Martínez, M.C. (coords.), Reconstruyendo la ciudad maya: el urbanismo en las sociedades antiguas: España, Sociedad Española de Estudios Mayas, 253–276.

Coe, R.S., 1967, The determination of paleo-intensities of the Earth's magnetic field with emphasis on mechanisms which could cause non-ideal behavior in Thellier's method: Journal of Geomagnetism and Geoelectricity, 19(3), 157–179. https://doi.org/10.5636/jgg.19.157

Constable, C., Korte, M., Panovska, S., 2016, Persistent high paleosecular variation activity in southern hemisphere for at least 10 000 years: Earth and Planetary Science Letters, 453, 78–86. https://doi.org/10.1016/j.epsl.2016.08.015

Day, R., Fuller, M., Schmidt, V.A., 1977, Hysteresis properties of titanomagnetites: Grain-size and compositional dependence: Physics of the Earth and Planetary Interiors, 13(4), 260–267. https://doi.org/10.1016/0031-9201(77)90108-X

Fanjat, G., Camps, P., Valdivia, L.A., Sougrati, M.T., Cuevas-Garcia, M., Perrin, M., 2013, First archeointensity determinations on Maya incense burners from Palenque temples, Mexico: New data to constrain the Mesoamerica secular variation curve: Earth and Planetary Science Letters, 363, 168–180. https://doi.org/10.1016/j.epsl.2012.12.035

García-Ruiz, R., Pérez-Rodríguez, N., Goguitchaichvili, A., Rodríguez-Ceja, M., Morales, J., Soler, A.M., Urrutia-Fucugauchi, J., 2021, On the absolute geomagnetic

http://dx.doi.org/10.18268/BSGM2025v77n2a200225

intensity fluctuations in Mexico over the last three millennia: Journal of South American Earth Sciences, 106, 102927. https://doi.org/10.1016/j.jsames.2020.102927

Gelman, A., Carlin, J.B., Stern, H.S., Rubin, D.B., 2013, Bayesian data analysis: New York, Chapman and Hall/CRC, 675 p. https://doi.org/10.1201/b16018

Gallareta, T.C., Castellanos, F.R., 2012, Las etapas más tempranas de la alfarería Maya en el noroeste de la Península de Yucatán: Ancient Mesoamerica, 23(2), 403–419. https://doi.org/10.1017/S0956536112000260

Goguitchaitchvili, A., Ruiz, R.G., Castillo, S.E., Morales, J., Ortiz, S., Fucugauchi-Urrutia, J. 2018a, Last two millenia Earth's magnetic field strength: new archaeointensity determinations from ichkaantijo, early to late maya classic period: Journal of Archaeological Science: Reports, 18, 292–299. https://doi.org/10.1016/j.jasrep.2018.01.023

Goguitchaichvili, A., Ruiz, R.G., Pavón-Carrasco, F.J., Contreras, J.J.M., Arechalde, A.M.S., Urrutia-Fucugauchi, J., 2018b, Last three millennia Earth's Magnetic field strength in Mesoamerica and southern United States: Implications in geomagnetism and archaeology: Physics of the Earth and Planetary Interiors, 279, 79–91. https://doi.org/10.1016/j.pepi.2018.04.003

Goguitchaichvili, A., Ortiz-Ruiz, S., Morales, J., Kravchinsky, V.A., de Lucio, O., Cejudo, R., García-Ruiz, R. Uc-González, E. Ruvalcaba, J.L., Pingarrón-Barba, L., 2020, Pyrotechnological knowledge in the pre-Hispanic Maya society: Magnetic and infrared spectrometry surveys of limekilns in the western Yucatan Peninsula (Mexico): Journal of Archaeological Science: Reports, 33, 102457. https://doi.org/10.1016/j.jasrep.2020.102457

Hervé, G., Perrin, M., Alva-Valdivia, L.M., Rodríguez-Trejo, A., Hernández-Cardona, A., Cordova Tello, M., Meza Rodriguez, C., 2019, Secular variation of the intensity of the geomagnetic field in Mexico during the first millennium BCE: Geochemistry, Geophysics, Geosystems, 20(12), 6066-6077. https://doi.org/10.1029/2019GC008668

Kirschvink, J.L., 1980, The least-squares line and plane and analysis of palaeomagnetic data: Geophysical Journal International, 62(3), 699–718. https://doi.org/10.1111/j.1365-246X.1980.tb02601.x

Lee, S.S., 1975, Secular variation of the intensity of the geomagnetic field during the past 3,000 years in north, central, and South America: U.S.A., The University of Oklahoma, doctoral thesis, 220 p.

Leonhardt, R., Heunemann, C., Krasa, D., 2004, Analyzing absolute paleointensity determinations: acceptance criteria and the software ThellierTool4.0: Geochemistry, Geophysics, Geosystems, 5(12), 1–11. https://doi.org/10.1029/2004GC000807

Mahgoub, A.N., Juárez-Arriaga, E., Böhnel, H., Siebe, C., Pavón-Carrasco, F.J., 2019, Late-Quaternary secular variation data from Mexican volcanoes: Earth and Planetary Science Letters, 519, 28–39. https://doi.org/10.1016/j.epsl.2019.05.001

Morales, J., Goguitchaichvili, A., Acosta, G., González-Moran, T., Alva-Valdivia, L., Robles-Camacho, J., Hernández-Bernal, M.S., 2009, Magnetic properties and archeointensity determination on Pre-Columbian pottery from Chiapas, Mesoamerica: Earth, Planets and Space, 61, 83–91. https://doi.org/10.1186/BF03352887

Nagata, T., Kobayashi, K., Schwarz, E.J., 1965, Archeomagnetic intensity studies of South and Central America: Journal of Geomagnetism and Geoelectricity, 17(3–4), 399–405.

Obando, L.G., Jimenez, S., Kussmaul, S., 2011, Petrographyc studies from mayan ceramics, Late Classic (600-900 ad), Chinikiha, Chiapas, Mexico: Revista Geológica de América Central, 44, 101–118.

Ortiz-Ruiz, S., García-Ruiz, R., Goguitchaichvili, A., de Lucio, O.G., Murguía Salazar, J.A., Vernet Tarragó, E., Góngora-Salas, A., Bautista, F., Morales-Contreras, J.J., 2024, Espectrometría infrarroja y datación arqueomagnética de un horno de cal en la periferia de Dzibilchaltún, Mérida, Yucatán: Boletín de la Sociedad Geológica Mexicana, 76(2), A170424. http://dx.doi.org/10.18268/BSGM2024v76n2a170424

Paterson, G.A., Tauxe, L., Biggin, A.J., Shaar, R., Jonestrask, L.C., 2014, On improving the selection of Thellier-type paleointensity data: Geochemistry, Geophysics, Geosystems, 15(4), 1180–1192. https://doi.org/10.1002/2013GC005135

Pavón-Carrasco, F.J., Rodríguez-González, J., Osete, M.L., Torta, J.M., 2011, A Matlab tool for archaeomagnetic dating: Journal of Archaeological Science, 38(2), 408–419. https://doi.org/10.1016/j.jas.2010.09.021

Pavón-Carrasco, F.J., Osete, M.L., Torta, J.M., De Santis, A., 2014, A geomagnetic field model for the Holocene based on archaeomagnetic and lava flow data: Earth and Planetary Science Letters, 388, 98–109. https://doi.org/10.1016/j.epsl.2013.11.046

Quiñones-Cetina, L., 2006, Del preclásico medio al clásico temprano: Una propuesta de fechamiento para el área nuclear de Izamal, Yucatán: Estudios de Cultura Maya, 28, 51–65.

Ramsey, C.B., 2009, Bayesian analysis of radiocarbon dates: Radiocarbon, 51(1), 337–360.

Rissolo, D., Rodríguez, J.M.O., Ball, J.W., 2005, A reassessment of the Middle Preclassic in northern Quintana Roo, in Shaw, J.M., Mathews, J.P. (eds.), Quintana Roo Archaeology: USA, University of Arizona Press, 66–76.

Rodríguez-Trejo, A., Alva-Valdivia, L.M., García-Amador, B.I., 2023, Paleomagnetism, rock magnetism and age determination of effusive and explosive Holocene volcanism in the Momotombo-Managua-Masaya region, Nicaragua: Journal of Volcanology and Geothermal Research, 437, 107792. https://doi.org/10.1016/j.jvolgeores.2023.107792

Rodríguez-Trejo, A., Böhnel, H., Ibarra-Ortega, H.E., 2024, LAPOD, Latin-American paleomagnetic online database: An online interface to access paleomagnetic data from Latin America: Journal of South American Earth Sciences, 145, 105060. https://doi.org/10.1016/j.jsames.2024.105060

Rogers, J., Fox, J.M.W., Aitken, M.J., 1979. Magnetic anisotropy in ancient pottery: Nature, 277, 644–646. https://doi.org/10.1038/277644a0

Schanner, M., Korte, M., Holschneider, M., 2022, ArchKalmag14k: A Kalman-filter based global geomagnetic model for the Holocene: Journal of Geophysical Research Solid Earth, 127(2), e2021JB023166. https://doi.org/10.1029/2021JB023166

Tauxe, L., Mullender, T.A.T., Pick, T., 1996, Potbellies, wasp-waists, and superparamagnetism in magnetic hysteresis: Journal of Geophysical Research: Solid Earth, 101(B1), 571–583. https://doi.org/10.1029/95JB03041

Tauxe, L., Bertram, H.N., Seberino, C., 2002, Physical interpretation of hysteresis loops: Micromagnetic modelling of fine particle magnetite: Geochemistry, Geophysics, Geosystems, 3(10), 1–22. https://doi.org/10.1029/2001GC000241

Tejero-Andrade, A., Cifuentes-Nava, G., Chávez-Segura, R.E., Hernández-Quintero, J.E., Argote-Espino, D.L., 2019, Experiences in the application of electric resistivity tomography (ert) 3-d in the archaeological site of Chichen Itza, Yucatan, in Symposium on the Application of Geophysics to Engineering and Environmental Problems 2019: Portland, Oregon, Society of Exploration Geophysicists and Environment and Engineering Geophysical Society, 238–247. https://doi.org/10.4133/sageep.32-054

http://dx.doi.org/10.18268/BSGM2025v77n2a200225

Thellier, E., Thellier, O., 1959, Sur l'intensite du shamp magnetique terrestre dans le passe historique et géologique: Annales de Geophysique, 15, 285–376.

Veitch, R.J., Hedley, I.G., Wagner, J.J., 1984, An investigation of the intensity of the geomagnetic field during roman times using magnetically anisotropic bricks and tiles: Archives des Sciences Geneve, 37(3), 359–373.